Nanoscale

Accepted Manuscript

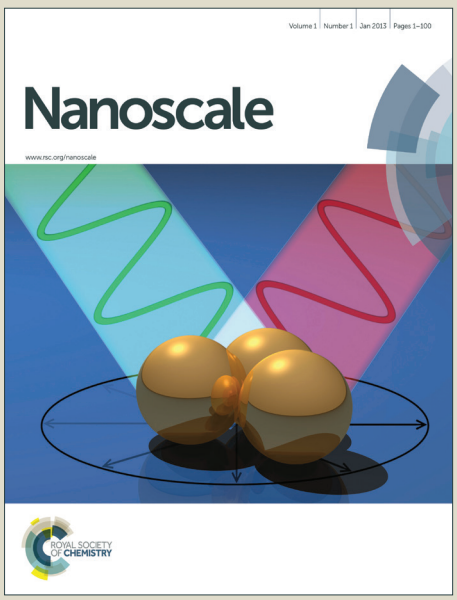

ROYAL SOCIETY OF CHEMISTRY

www.rsc.org/nanoscale

Journal Name

COMMUNICATION

Tuning and Understanding the Phase Interface of TiO_2 Nanoparticles for More Efficient Lithium Ion Storage†

Received 00th January 20xx,
Accepted 00th January 20xx

DOI: 10.1039/x0xx00000x

www.rsc.org/

Rui Wang, ‡[a] Xuyan Xue, ‡[a] Wencai Lu,[a] Hongwei Liu,[b] Chao Lai,[c] Kai Xi,*[d] Yanke Che,[e] Jingquan Liu,[a] Shaojun Guo*[f] and Dongjiang Yang*[a]

We demonstrate that mixed-phase anatase-TiO_2(B) nanoparticles can provide an interesting interphase interface with atomic-level contact for achieving more efficient Li ion storage with high capacity and cycle life. A novel lithium storage mode - "interfacial charge storage in allomorphs" (ICSA)- plays an important role in enhancing Li ion storage.

Transition metal oxide nanoparticles (TMO NPs) have been widely investigated as anode materials for lithium ion batteries (LIBs) because they show the obvious advantages in shortening Li^+ ions diffusion distance, and reducing the volume expansion/contraction during continuous charge/discharge process due to their large surface area and good conductivity.[1-6] Recent studies reveal that the interface of TMO NPs and another assistant materials (*e.g.* nanostructured metal/Li_2O composite) can provide the additional Li ion storage, in which Li ions are stored on Li_2O side of the interface and electrons are localized on the metal side, leading to a strong charge separation and thus the enhanced Li ion storage.[7-9] Therefore, creating the more efficient interface between two materials will be very important for achieving high-performance lithium ion storage. However, the biggest challenge of creating the interface by use of two immiscible materials is that the interface contact is still very limited, which is not suitable for maximizing the lithium ion storage.[10-13] In this regard, the rational design of interphase interface with atomic-level contact by the use of individual nanomaterials may provide the best choice for maximizing the lithium ion storage.

It is known that mainly TiO_2 exists in four polymorphs: anatase, rutile, brookite and TiO_2(B). The structure of anatase can be considered as a stacking of one dimensional zigzag chains consisting of distorted edge-sharing TiO_6 octahedra, which provides empty zigzag channels for Li^+ insertion to form $LixTiO_2$. Therefore, anatase phase is generally used as host for solid-state diffusion of Li^+. TiO_2 (B) can also be employed as anode materials for LIBs because of its structure particularity. The ideal TiO_2(B) is composed of corrugated sheets of edge- and corner-sharing TiO_6 octahedrals. In this special framework, TiO_2(B) possesses one-dimensional parallel infinite channels, providing more open structure than other polymorphs. The diffusion of Li^+ in TiO_2(B) is a pseudocapacitive faradic process, which is faster than that in anatase.[14,15] Considering these, creating the interesting atomic-level phase interface between anatase and TiO_2(B) may provide new opportunity for achieving more efficient lithium ion storage. We recently demonstrated that TiO_2 NPs with the mixed TiO_2(B) and anatase phases could form the firm connection at surface and interface *via* crystallographic similarity of two different nanocrystals, instead of a random aggregation of two crystals in allomorphic NPs.[16-18] This indicates that the maximized Li ion storage might be achieved at the phase boundaries of allomorphic TMO NPs. Another unanswered question for allomorphic TMO NPs for lithium ion storage is that the accurate Li storage behaviour at the phase interface (crystal interface or interphase boundaries) in allomorphic TMO anode materials is still hard to be determined because the preferred orientation and interfaces between the crystals of different phases in mixed phase materials are extremely difficult to determine.

Herein, we demonstrate a new concept that TiO_2 NPs with mixed TiO_2(B) and anatase phases, prepared from protonated titanate ($H_2Ti_3O_7$) nanosheets/graphene composite (denoted as T(AB)/G) can have the interesting interphase interface for achieving more efficient Li ion storage with high capacity and cycle life. In our previous work,[19-22] based on the phase

[a] Collaborative Innovation Centre for Marine Biomass Fibers, Materials and Textiles of Shandong Province; College of Chemical and Environmental Engineering, Qingdao University, Qingdao, P R China. E-mail: d.yang@qdu.edu.cn.
[b] Australian Centre for Microscopy and Microanalysis (ACMM), the University of Sydney, Sydney, NSW 2006, Australia.
[c] School of Chemistry and Chemical Engineering, Jiangsu Normal University, Xuzhou, Jiangsu 221116, China.
[d] Department of Materials Science and Metallurgy University of Cambridge, Cambridge, UK. E-mail: kx210@cam.ac.uk.
[e] Institute of Chemistry, The Chinese Academy of Sciences, Beijing, P R China.
[f] Physical Chemistry and Applied Spectroscopy, Los Alamos National Laboratory, Los Alamos, New Mexico 87545, USA. E-mail: sguo@lanl.gov; shaojun.guo.nano@gmail.com
‡ These authors contributed equally to this work.
† Electronic Supplementary Information (ESI) available: detailed synthesis procedure, tables, TEM, FTIR data, and XRD results. See DOI: 10.1039/x0xx00000x

transformation invariant line strain (ILS) theory and high-resolution transmission electron microscopy (HRTEM) investigation, we have determined that (001) plane of anatase phase has the same orientation with (100) plane of TiO_2(B) phase, hence the (010) plane of anatase can extend across into the adjacent TiO_2(B) phase. The determined interphase interface provides a very good opportunity to observe the novel interfacial Li storage behaviour in mixed phase TiO_2 anode materials. Indeed, herein we found such interphase interface allows T(AB)/G exhibit higher performance for LIBs in the term of capacity and cycle life than those of the pure anatase (T(A)/G) and pure TiO_2(B) (T(B)/G) anodes. The first-principles simulations based on density-functional theory (DFT) shows a new charge separation mechanism- "interfacial charge storage in allomorphs" (ICSA)-should be responsible for the additional Li storage at the phase interface between the anatase and TiO_2(B), in which the dominant Ti atoms on (001) plane of anatase are beneficial for accepting electrons, followed by the conversion of Ti^{4+} into Ti^{3+} and the Li^+ ions can be accommodated on the (100) plane of TiO_2(B), which is occupied by O atoms. Therefore, the separation of Li^+ ions and electrons finally results in a reduction of recombination between the Li^+ ions and the electrons.

In order to prove our concept, T(AB)/G was prepared as follows (Fig. 1a). $H_2Ti_3O_7$ nanosheets were first synthesized from $TiOSO_4$ by a hydrothermal reaction (see the details in the experimental section), and then modified with (3-aminopropyl) triethoxysilane (APTES) coupling agent to graft -NH_2 groups on the $H_2Ti_3O_7$ nanosheets (proved by the infrared spectroscopy of Fig. S1). Then, 1-pyrenebutyric acid (PA) on $H_2Ti_3O_7$ nanosheets was used to react with the grafted -NH_2 groups to distribute four fused benzene rings onto the surface of $H_2Ti_3O_7$ nanosheets. Subsequently, the modified $H_2Ti_3O_7$ nanosheets could automatically attach to the G layers *via* strong π-π stacking interactions (proved by the infrared spectroscopy of Fig. S2). Finally, the as-prepared hybrids were calcined at 600 °C in a N_2 atmosphere, leading to T(AB)/G. For the comparison, the as-prepared hybrids was also carried out at 300 and 700 °C to obtain pure TiO_2(B) (T(B)/G) and anatase (T(A)/G) anodes, respectively.

X-ray diffaction (XRD) technique was used to detect the phase-transition process. Fig. 1b and Fig. S3 show the XRD pattern of as-prepared TiO_2/G NPs, $H_2Ti_3O_7$/G and $H_2Ti_3O_7$ nanosheets. The diffraction peaks of anatase (JCPDS 21-1272) and TiO_2(B) (JCPDS 74-1940) were observed, indicating that the $H_2Ti_3O_7$ nanosheets were fully converted to TiO_2 NPs with mixed anatase and TiO_2(B) phases. The phase transformation was also proved by Raman spectra of the TiO_2/G NPs composite (Fig. 1c). The peaks representing Ti-O vibration of both anatase and TiO_2(B) crystals were in good agreement with the XRD result. In addition to phonon modes arising from the TiO_2, two broad peaks at about 1342 and 1592 cm−1 were observed in the Raman spectra (the inset in Fig. 1c), assigned to the D (defect-related) peak and the G (graphitic, sp^2) peak of the graphene.[23-25] This indicates that the TiO_2 NPs were attached on the G.

The N_2 absorption-desorption isotherms of T(AB)/G, T(A)/G and T(B)/G (Fig. 2a and Table S1) exhibit the type IV isotherms with type H1 hysteresis loop according to IUPAC,[26-28] and

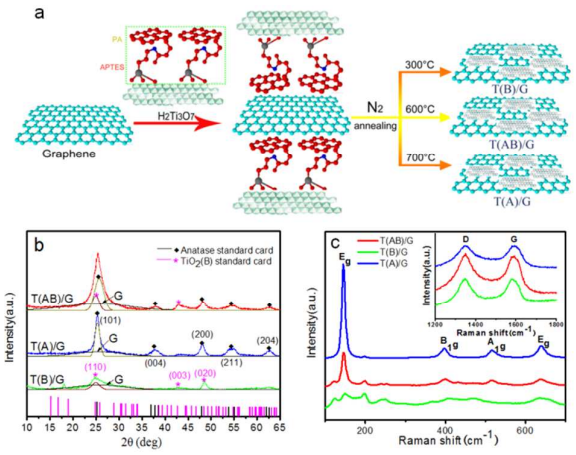

Fig. 1 (a) Schematic illustration for the preparation ofTiO_2/graphene. (b) XRD patterns and (c) Raman spectroscopy of T(B)/graphene, T(AB)/graphene and T(A)/graphene nanosheets.

display their similar high specific surface area (144-171 $m^2\ g^{-1}$), large pore volumes (0.48-0.55 $cm^3\ g^{-1}$), and narrow pore size distributions (Table S1). The pore size distributions, obtained from the Barrett–Joyner–Halenda (BJH) method, are shown in Fig. 2b. They contain two types of the pores, in which the small pores (at ~3.8 nm) are attributed to agglomeration of the graphene nanosheets,[29,30] and the mesopore with sizes at ~10.0 nm is assigned to the random aggregation of TiO_2 NPs.[31]

The microstructure of the $H_2Ti_3O_7$/G hybrid before and after thermal treatment was characterized by using transmission electron microscopy (TEM). As shown in Fig. 3a, the $H_2Ti_3O_7$ nanosheets are overlaid on the top of G. The selected area electron diffraction (SAED) spots of $H_2Ti_3O_7$/G hybrids in Fig. 3b show two sets of spots, which can be indexed to the (0002) and $(10\bar{1}0)$ planes of G, and the (200), (011), (213) and (223) planes of $H_2Ti_3O_7$ phase, respectively. Fig. 3c-f shows the energy dispersive spectroscopy (EDS) mapping of of Ti (green), O (blue), and C (red), proving $H_2Ti_3O_7$ are formed on the surface of G. Furthermore, the high-resolution TEM (HRTEM) image (Fig. 3g) of $H_2Ti_3O_7$/G hybrids shows a set of lattice fringes with a spacing of 0.23 nm, corresponding to the $(10\bar{1}0)$ plane of G and another set of lattice fringes with a spacing of 0.19 and 0.20 nm, attributed to both (020) and (203) planes of $H_2Ti_3O_7$.

After the thermal treatment at 600 °C, highly crystalline TiO_2 NPs were observed on the graphene surface (Fig. 4a). The SAED spots of TiO_2/G hybrids (Fig. 4b) show three sets of spots, which can be indexed to the $(\bar{2}110)$ and $(10\bar{1}0)$ planes of G, the (101), (200) and (120) planes of anatase phase, and the (110), (203), (600), (113) and (424) planes of TiO_2(B) phase.

This further indicates that the parent $H_2Ti_3O_7$ nanosheets were converted to the mixed phase anatase/TiO_2(B) NPs after calcination at 600 °C. The HRTEM image in Fig. 4c provides more subtle structure of the mixed phase anatase/TiO_2(B) NPs

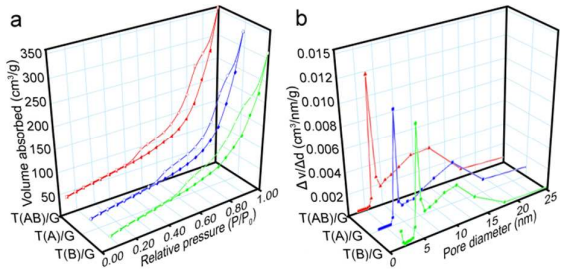

Fig. 2 (a) N_2 adsorption and desorption isotherm and (b) the pore size distribution of T(AB)/G, T(A)/G and T(B)/G.

along the $[1\bar{1}1]$ direction of anatase phase. A set of lattice fringes with a spacing of 0.57 nm, corresponding to the (200) plane of TiO_2(B) and another set of lattice fringes with a spacing of 0.35 nm, attributed to both (011) and (101) planes of anatase phase were observed. The Inversed Fast Fourier Transform (IFFT) image of the region enclosed by a rectangle in Fig. 4c reveals the exist of phase interface between the adjacent TiO_2(B) and anatase nanocrystals (Fig. 4d). Apparently, the (010) planes of anatase NPs have a basal spacing of 0.378 nm, close to that of the (010) planes (0.374 nm) of the adjacent TiO_2(B) NPs. With (001) plane of anatase parallel to (100) plane of TiO_2(B), the (001) plane of anatase and the (100) plane of TiO_2(B) have the same orientation so that the(010) plane of anatase extends across into the adjacent TiO_2(B) phase. This observation is in good agreement with our previous finding (different TiO_2 nanostructures),[18] where anatase and TiO_2(B) phases in a single TiO_2 nanofiber should be combined coherently with a close crystallographic registry to reduce the Coulomb forces and minimize the dangling bonds. Furthermore, Fig. 4e-h shows the EDS mapping of TiO_2/G hybrids. It is obvious that TiO_2 NPs are formed on the surface of G. The microstructures of T(B)/G and T(A)/G samples were also recorded in Fig. S4 and S5, where only pure TiO_2(B) or anatase TiO_2 NPs was observed on graphene layers.

To demonstrate the effects of mixed phase structure on the Li-ion insertion/extration properties, T(AB)/G, T(A)/G and T(B)/G electrodes were fabricated as follows. The working electrodes were prepared by casting a mixture of the active materials, acetylene black, and binder(polytetrafluoroethylene, PTFE) in a weight ratio of 75: 15: 10 onto pure Cu foil. Fig. 5a shows the discharge/charge profiles of three types of TiO_2 electrodes from the voltage 3.0 to 1.0 V *vs* Li/Li^+. Apparently, during the initial discharge and charge processes, the capacity of the T(AB)/G electrode can achieve at 164 and 143 mA h g^{-1}, corresponding to a Coulombic efficiency (CE) of 88%, which are better than those of T(B)/G (157 and 130 mA h g^{-1}, corresponding to a CE of 83%) and T(A)/G (146 and 124 mA h g^{-1}, corresponding to a CE of 85%), respectively. This value is better than those of pure phase T(B)/G (15%) and T(A)/G electrodes (17%). The irreversible capacity of 21 mAh g^{-1}(12%) was mainly attributed to electrolyte reductive decomposition, forming solid electrolyte interphase layer on the electrode surface in the initial discharging step.[31]

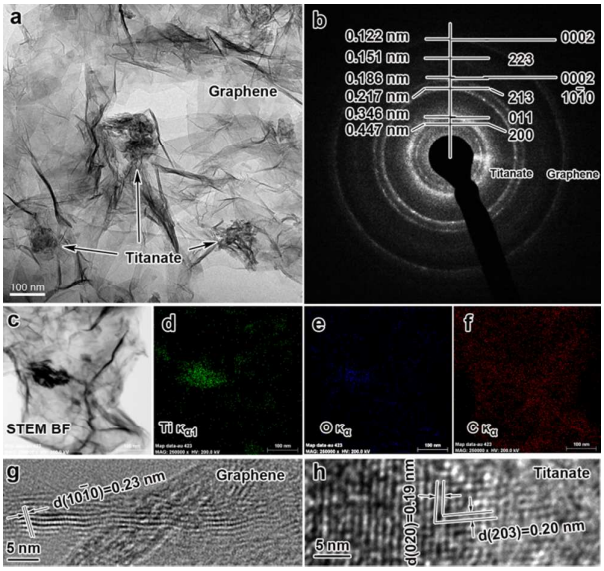

Fig. 3 (a) TEM image, (b) SAED pattern, (c) STEM DF image, (d-f) elemental mapping and (g-h) HRTEM images of H-titanate/G nanohybrids

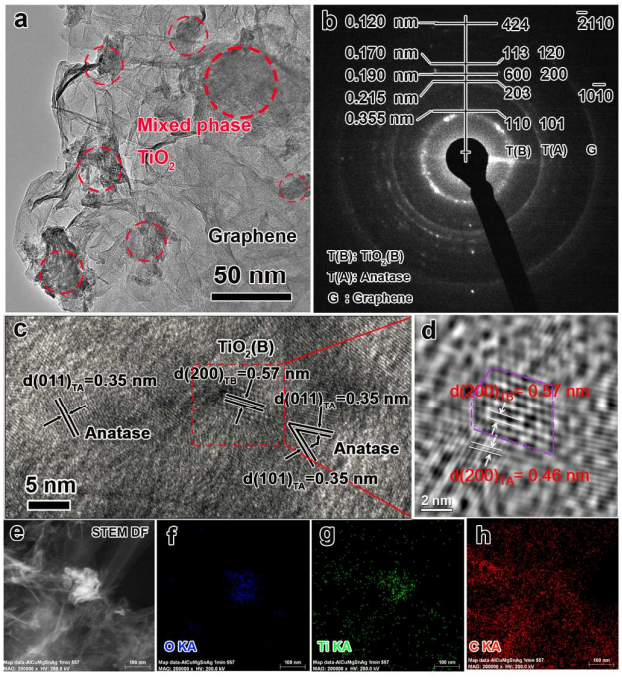

Fig. 4 (a) TEM image, (b) SAED pattern, (c) HRTEM image, (d) IFFT image of the selected area in plane c, (e) STEM dark-field (DF) image, (f-h) elemental mapping of oxygen, titanium and carbon of T(AB)/G nanohybrids.

Clearly, the mixed phase T(AB)/G electrode exhibited the better specific capacity and irreversibility during the electrochemical lithium insertion/extraction.

Furthermore, the discharge capacities of the TiO_2/G electrodes decrease almost linearly in the first 5 cycles and then are stabilized over the remaining cycles (Fig. 5b). After 40 galvanostatic cycles at a high current density of 1000 mA g^{-1}, the discharge capacities of T(AB)/G, T(A)/G and T(B)/G electrodes were stabilized to be around 134, 123, and 109 mA h g^{-1}, respectively. The capacity losses of T(AB)/G, T(A)/G and T(B)/G electrodes were 15.8, 18.7, and 30.5%, respectively. Obviously, the mixed phase T(AB)/G exhibits better cycling stability in comparison with the pure phase samples. Fig. 5c shows the rate capability of the three electrodes. T(AB)/G shows much better rate ability with the specific discharge capacity being around 164 (1 C), 154 (2 C), 141 (4 C), 135 (6 C) and 130 mA h g^{-1} (8 C), respectively than the T(A)/G electrode (143, 127, 116, and 106 mA h g^{-1} at the same current densities) and T(B)/G electrode (122, 105, 93, and 82 mA h g^{-1} at the same current densities). That means the the mixed phase T(AB)/G electrode exhibits the best capacity retention at high discharge/charge rate, indicating that the mixed phase structure of T(AB)/G facilitates the fast Li-ion diffusion and high electron transport. As a comparison, the T(AB)/G exhibits much better rate capability than the pure T(AB) nanosheets (see Fig. S6). This is because the graphene can improve the electron conductivity of TiO_2 and thus improve the rate capability. Given T(AB)/G, T(A)/G, and T(B)/G show the similar crystallite size and specific surface area, we think that the size and surface area should be not responsible obvious difference between the mixed phase T(AB)/G and for the difference on lithium storage ability for these three samples. The most the pure phase T(A)/G (or T(B)/G) is the phase interface between anatase and TiO_2(B) in T(AB)/G. Specifically, the (001) plane of anatase and the (100) plane of TiO_2(B) have the same orientation to connect the anatase and TiO_2(B) together tightly. Herein, a novel interfacial charge storage in allomorphs (ICSA) was proposed to explain the origin of higher performance of mixed phase TiO_2(B)/anatase anode in lithium storage. The (100) plane of TiO_2(B) is occupied by O atoms only (Fig. 6a), and the dominated atoms at the (001) plane of anatase are Ti atoms (Fig. 6b). The delicate atomic arrangement at the phase interface between TiO_2(B) and anatase can facilitate an additional Li storage *via* the charge separation. As depicted in Fig. 6c, the Ti atoms at the (001) plane of anatase act as acceptor to capture electrons, followed by the conversion of Ti^{4+} into Ti^{3+}.[33,34] Meanwhile, besides the insert in the parallel tunnels perpendicular to the (010) plane of the TiO_2(B) phase, the Li^+ ions can be accommodated on the (100) plane of TiO_2 (B), which is occupied by O atoms. Therefore, the separation of Li^+ ions and electrons results in a reduction of recombination between the Li^+ ions and the electrons, leading to the enhanced specific capacity and rate performance of the mixed phase electrode.

To verify the ICSA mechanism, we carried out the first-principles calculations based on density-functional theory (DFT) using a model slab with TiO_2(B) layer and anatase layer. The two-dimensional slab contains several layers of Ti-terminated anatase and O-terminated TiO_2(B), respectively. The first-principles simulations of the Li storage in the TiO_2(B)/anatase interface are performed within the local density approximation and ultrasoft pseudopotential method in the CASTEP code.[35] The energy cutoff for plane wave basis is 450 eV and the k-point for the slab is 5 × 3 × 1. The leftmost layer atoms of T(A) and the rightmost layer atoms of T(B) were fixed to their positions in bulk T(A) or T(B) when the slab was optimized. We located a Li atom on various sites of T(B), and found that the tunnel T1 site is more stable for Li ion storage than the tunnel T2 sites (green zone in Fig. 6d&e). According to the present model, the Li^+ ions would be stored on the T(B) side of the interface, while there is an electron transfer from the Li-doped T(B) to T (A), resulting in a charge separation.

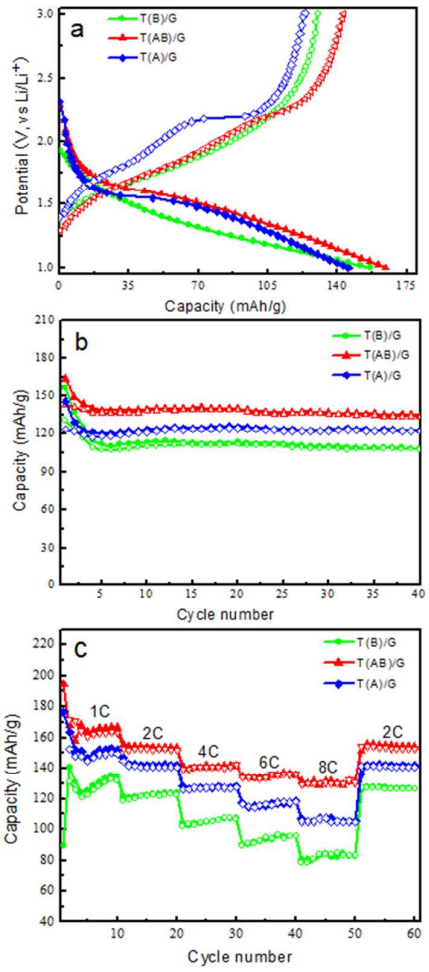

Fig. 5 (a) Charge/discharge profiles for T(B)/G, T(AB)/G and T(A)/G nanosheets between 1.0 to 3.0 V at a current density of 1000 mA g−1 at room temperature, (b) Cycling performance of T(B)/G, T(AB)/G and T(A)/G nanosheets to 40 cycles at 1000 mA g−1 charge/discharge rate, (c) Specific capacity of nanosheets at different C rates: 1 C, 2 C, 4 C, 6 C, and 8 C (1C = 335 mA g−1, open: charge, solid: discharge).

Using the optimized structure of the T(A)/T(B) interface, we calculated the Mulliken charge distributions in both the slabs with and without the Li-doping interface. The charges of the T(A)/T(B) interface atoms were obtained, as listed in Table 1. The extra Li atom considered as an electron donor loses 1.33*e*. On the T(A) (001) double-atom layer, there is an average increase of electrons of ~ 0.16*e* on the Ti atom and ~ 0.03e on the O atom. Therefore, the T(A) interface layer can serve as an electron acceptor. Meanwhile, on the T(B) (100) interface layer, there is also an average increase of electrons of ~ 0.2*e* on the Ti atom and ~ 0.09*e* on the O atom. However, Li^+ is also located at the side of T(B). Therefore, the T(B) and Li lose electrons as a whole, and the T(A) gains electrons, resulting in a charge separation at the T(A)/T(B) interface. This result is in

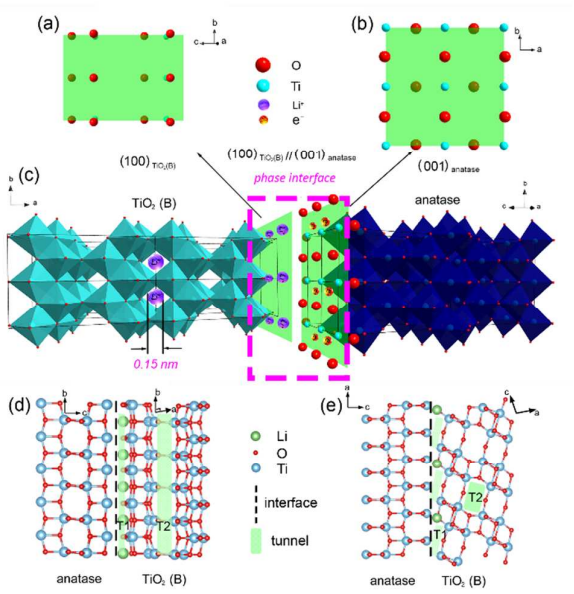

Fig. 6 A proposed interfacial storage model in mixed phase TiO_2(B)/anatase system: (a) 2-D atomic profile of (100) plane of TiO_2(B). (b) 2-D atomic profile of (001) plane of anatase. (c) Charge separation at the phase interface between TiO_2(B) and anatase crystals. Optimized atomic arrangement of the model slab with Li atom in the interface between TiO_2(B) and anatase phase: (d) View along [100] direction of anatase and [001] direction of TiO_2(B), (e) View along [010] direction of anatase and TiO_2(B).

Table 1 Mulliken charge distribution for TiO_2(B)/anatase interface with and without Li atom insertion.

Slab	Interfacial Li	O-av[a]	Ti-av[a]	Doped Li[b]
TiO_2(B)	undoped	-0.64	1.06	/
TiO_2(B)	doped	-0.73	0.86	1.33
Anatase	undoped	-0.66	0.91	/
Anatase	doped	-0.69	0.75	/

[a]O-av and Ti-av are average effective charge per atom on O and Ti atom in the interface layer of TiO_2(B) and TiO_2(A). [b]Doped Li is effective charge on lithium per atom.

Good agreement with the proposed ICSA mechanism. Furthermore, a typical Nyquist plot of T(AB)/G, T(A)/G, T(B)/G and T(AB) electrodes was given in Fig. S7. Obviously, T(AB)/G displays the lowest resistance, further supporting our ICSA mechanism.

To summarize, we demonstrate a multi-step process for the controlled synthesis of T(AB)/G through annealing the $H_2Ti_3O_7$/G composite nanosheets in N_2 at high temperature, which provide an interesting interphase interface with atomic-level contact for achieving more efficient Li ion storage with high capacity and cycle life. We found that the mixed phase T(AB) exhibits higher specific capacity and better rate performance than those of the pure T(A) and T(B). The high-performance Li ion storage ability of the mixed phase electrode should be ascribed to the additional Li storage at the phase interface between the T(B) and T(A) (novel ICSA mechanism). This has been well verified by the first-principles calculations based on DFT, in which the interfacial (001) plane of anatase acts as acceptor to capture electrons, and the (100) plane of TiO_2 (B), occupied by O atoms can accommodate theLi^+ ions. The proposed ICSA mechanism open a new avenue for tuning and understanding new multi-phase materials for future more efficient LIBs.

Acknowledgements

This work was supported by the National Natural Science Foundation of China (No.21207073 and 51173087) and Australia Research Council Discovery Project (No 130104759).

Notes and references

1 S. M. Hwang, Y. G. Lim, J. G. Kim Y. U. Heo, J. H. Lim, Y. Yamauchi, M. S. Park, Y. J. Kim, S. X. Dou and J. H. Kim, *Nano Energy*, 2014, **10**, 53.
2 G. Jeong, J. G. Kim, M. S. Park, M. S., S. M. Hwang, Y.U. Kim,Y. J. Kim, J. H. Kim and S. X. Dou, *ACS Nano.*, 2014, **3**, 2977.
3 J. W. Deng, C. L. Yan, L. C. Yang, S. Baunack, S. Oswald, H. Wendrock, Y. F. Mei and O. G. Schmidt, *ACS Nano.*, 2013, **7**, 6948.
4 Y. M. Sun, X. L. Hu, W. Luo and Y. H. Huang, *ACS Nano.*, 2011, **5**, 7100.
5 G. M. Zhou, D. W. Wang, F. Li, L. L. Zhang, N. Li, Z. S. Wu, L. Wen, G. Q. Lu and H. M. Cheng, *Chem. Mater.*, 2010, **22**, 5306.
6 J. G. Kim, M. S. Park, S. M. Hwang, Y. U. Heo, T. Liao, Z. Sun, J. H. Park, K. J. Kim, G. Jeong, Y. J. Kim, J. H. Kim and S. X. Dou, *ChemSusChem,* 2014, **7**, 1451.
7 J. Y. Shin, D. Samuelis and J. Maier, *Adv. Funct. Mater.*, 2011, **21**, 3464.
8 M. D. Rahman, J. Z. Wang, M. F. Hassan, D. Wexler and H. K. Liu, *Adv. Energy Mater.*, 2011, **1**, 212.
9 Y. Zhukovskii, P. Balaya, E. Kotomin and J. Maier, *Phys. Rev. Lett.*, 2006, **96**, 058302.
10 Q. L. Wu, J. G. Xu, X. F. Yang, F. Q. Lu, S. M. He, J. L. Yang, H. J. Fan and M. M. Wu, *Adv. Energy Mater.*, 2014, **5**, 1401756.
11 Z. Q. Niu, L. L. Liu, L. Zhang, Q. Shao, W. Y. Zhou, X. D. Chen and S. S. Xie, *Adv. Mater.*, 2014, **26**, 3681.

12 Y. X. Tang, Y. Y. Zhang, J. Q. Deng, J. Q. Wei, H. L. Tam, B. K. Chandran, Z. L. Dong, Z. Chen and X. D. Chen, *Adv. Mater.*, 2014, **26**, 6111.
13 Y. X. Tang, Y. Y. Zhang, J. Y. Deng, D. P. Qi, W. R. Leow, J. Q. Wei, S. Y. Yin, Z. L. Dong, R. Yazami, Z. Chen and X. D. Chen, *Angew. Chem. Int. Ed.*, 2014, **126**, 13706.
14 X. Su, Q. L. Wu, X. Zhan, J. Wu, S. Y. Wei and Z. H. Guo, *J. Mater. Sci.*, 2012, **6**, 2519.
15 Z. G. Yang, D. Choi, S. Kerisit, K. Rosso, D. H. Wang, J. S. Zhang, G. Graff and J. Liu, *J. Power Sources*, 2009, **2**, 588.
16 H. W. Liu, Z. F. Zheng, D. J. Yang, X. B. Ke, E. Jaatinen, J. Zhao and H. Y. Zhu, *ACS Nano.*, 2010, **4**, 6219.
17 Q. L. Wu, J. G. Xu, X. F. Yang, F. Q. Lu, S. M. He, J. L. Yang, H. J. Fan and M. M. Wu, *Adv. Energy Mater.*, 2015, **5**, 1401756.
18 J. J. Li, D. J. Yang, X. Y. Zhu, L. Wang, A. Umar, G. J. Song, *Sci. Adv. Mater.*, 2015, **7**, 821.
19 D. J. Yang, H. W. Liu, Z. F. Zheng, Y. Yuan, J. C. Zhao, E. R. Waclawik, X. B. Ke and H. Y. Zhu, *J. Am. Chem. Soc.,* 2009, **131**, 17885.
20 D. J. Yang, J. Zhao, H. W. Liu, Z. F. Zheng, M. O. Adebajo, H. X. Wang, X. T. Liu, H. J. Zhang, J. C. Zhao, J. Bell and H. Y. Zhu, *Chem. Eur. J.*, 2013, **19**, 5113.
21 L. Zhang, D. W. Jing, X. L. She, H. W. Liu, D. J. Yang, Y. Lu, J. Li, Z. F. Zheng and L. J. Guo, *J. Mater. Chem. A*, 2014, **2**, 2071.
22 S. C. Zhang, D. J. Yang, D. W. Jing, H. W. Liu, L. Liu, Y. Jia, M. H. Gao, L. J. Guo, Z. Y. Huo, *Nano Res.*, 2014, **7**, 1659.
23 L. F. Shen, X. G. Zhang, H. S. Li, C. Z. Yuan and G. Z. Cao, *J. Phys. Chem. Lett.*, 2011, **2**, 3096.
24 J. X. Zhu, D. Yang, Z. Y. Yin, Q. Y. Yan and H. Zhang, *Small*, 2014, **10**, 3480.
25 Y. H. Zhu, W. Liu, X. Y. Zhang, J. C. He, J. T. Chen, Y. P. Wang and T. B. Cao, *Langmuir*, 2013, **29**, 744.
26 R. Mukherjee, A. Thomas, A. Krishnamurthy and N. Koratkar, *ACS Nano.*, 2012, **6**, 7867.
27 S. Brunauer, L. S. Deming, W. Deming and E. Teller, *J. Am. Chem. Soc.*, 1940, **62**, 1723.
28 R. Schmidt, M. Stocker, E. Hansen, D. Akporiaye and O. H. Ellestad, *Micropor. Mater.*, 1995, **3**, 443.
29 B. Sun, B. Wang, D. W. Su, L. D. Xiao, H. J. Ahn and G. X. Wang, *Carbon*, 2012, **50**, 727.
30 Q. Cheng, J. Tang, J. Ma, H. Zhang, N. Shinya and L. C. Qin, *Phys. Chem. Chem. Phys.*, 2011, **13**, 17615.
31 X. Zhang, P. S. Kumar, V. Aravindan, H. H. Liu, J. Sundaramurthy, S. G. Mhaisalkar, H. M. Duong, S. Ramakrishna and S. Madhavi, *J. Phys. Chem. C*, 2012, **116**, 14780.
32 F. Zhang, H. Q. Cao, D. M. Yue, J. X. Zhang and M. Z. Qu, *Inorg. Chem.,* 2012, **51**, 9544.
33 D. H. Wang, J. Li, Z. G. Yang, Z. M. Nie, R. Kou, D. H. Hu, C. M. Wang, L. V. Saraf, J. G. Zhang, I. A. Aksay and J. Liu, *ACS Nano*., 2009, **3**, 907.
34 J. X. Qiu, P. Zhang, M. Ling, S. Li, P. R. Liu, H. J. Zhao and S. Q. Zhang, *ACS Appl. Mater. Inter.*, 2012, **4**, 3636.
35 A. L. M. Reddy, A. Srivastava, S. R. Gowda, H. Gullapalli, M. Dubey and P. M. Ajayan, *ACS Nano.*, 2010, **4**, 6337.